ADVANCES IN ATMOSPHERIC SCIENCES, VOL. 29, NO. 6, 2012, 1200–1213

Projections of the East Asian Winter Monsoon under the IPCC AR5 Scenarios Using a Coupled Model: IAP_FGOALS

WEI Ke*[1] (魏 科) and BAO Qing[2] (包 庆)

[1] *Center for Monsoon System Research, Institute of Atmospheric Physics, Chinese Academy of Sciences, Beijing* 100080

[2] *State Key Laboratory of Numerical Modeling for Atmospheric Sciences and Geophysical Fluid Dynamics, Institute of Atmospheric Physics, Chinese Academy of Sciences, Beijing* 100029

(Received 5 November 2011; revised 16 February 2012)

ABSTRACT

Responses of the East Asian winter monsoon (EAWM) in future projections were studied based on two core future projections of CMIP5 in coordinated experiments with the IAP-coupled model FGOALS2-s. The projected changes of EAWM in climatology, seasonality, and interannual variability are reported here; the projections indicated strong warming in winter season. Warming increased with latitude, ranging from 1°C to 3°C in the Representative Concentration Pathways simulation RCP4.5 projection (an experiment that results in additional radiative forcing of ∼4.5 W m^{-2} in 2100) and from 4°C to 9°C in the RCP8.5 projection (an experiment that results in additional radiative forcing of ∼8.5 W m^{-2} in 2100). The northerly wind along the East Asian coastal region became stronger in both scenarios, indicating a stronger EAWM. Accordingly, interannual variability (described by the standard deviation of temperature) increased around the South China Sea and lower latitudes and decreased over eastern China, especially in North China. The two EAWM basic modes, defined by the temperature EOF analysis over East Asia, were associated with the Arctic Oscillation (AO) and stratospheric polar vortex. The future projections revealed more total variance attributable to the secondary mode, suggesting additional influences from the stratosphere. The correlation between AO and the leading mode decreased, while the correlation between AO and the secondary mode increased, implying increased complexity regarding the predictability of EAWM interannual variations in future projections.

Key words: East Asian winter monsoon, CMIP, AO, stratospheric polar vortex, FGOALS

Citation: Wei, K., and Q. Bao, 2012: Projections of the East Asian winter monsoon under the IPCC AR5 scenarios using a coupled model: IAP_FGOALS. *Adv. Atmos. Sci.*, **29**(6), 1200–1214, doi: 10.1007/s00376-012-1226-5.

1. Introduction

As one of the most energetic circulation components of the global climate system, the anomalies in the East Asian winter monsoon (EAWM) usually cause excessive damage and large economic loss to the densely populated East Asia. For example, the unusual EAWM in February 2008 caused extremely low temperatures, blizzards, and freezing rain over large region of southern China. The economic losses were estimated at ∼$ 25 billion and 129 casualties were incurred (Gu et al., 2008; Tao and Wei, 2008; Zhou et al., 2009; Bao et al., 2010a). The winter monsoon is also closely related to other climate systems, such as convection and SSTs near the Maritime Continent (Chang et al., 1979; Bueh and Ji, 1999), climate in North America (Cohen et al., 2001; Yang et al., 2002), ENSO evolution, intensity, and periodicity (Lau and Chang, 1987; Huang et al., 2004; Li et al., 2007), and the Asian summer monsoon (EASM) (Sun and Sun,

*Corresponding author: WEI Ke, weike@mail.iap.ac.cn

1994; Chen et al., 2000; Yan et al., 2011). Therefore, understanding EAWM anomalies and the ability to predict them is very meaningful and even imperative.

The climate system model has become a useful tool to simulate past climate anomalies and to project future climate changes. Therefore, we used a climate system model to investigate changes in the EAWM in the future. Several studies on the projection of EAWM are available (e.g., Hu et al., 2000; Bueh, 2003; Jiang et al., 2010); however, compared to its summer counterpart, much less research has been devoted to understanding the EAWM under future scenarios.

Since the Intergovernmental Panel on Climate Change (IPCC) Fourth Assessment Report (AR4), a new generation of scenarios has been recommended for the projections of emissions, evaluation of climate change, adaptation, and vulnerability and response strategies. These new scenarios updated the previous ones mainly in their combination of the new economic data, information about emerging technologies and high-resolution observations of changing environmental factors such as land use and land cover. This subsequent set of forcing agents will be widely used in the upcoming IPCC Fifth Assessment Report (AR5). Modeled projections are Representative Concentration Pathways scenarios (RCP experiments; Taylor et al., 2009; Moss et al., 2010). Therefore, the projected EAWM changes should be revaluated using the updated scenarios and compared with previous studies.

With the latest version of IAP (Institute of Atmospheric Physics) atmosphere–land–ocean coupled climate system model, the projections of a new coordinated climate model called CMIP5 (the Fifth Coupled Model Intercomparison Project, which will be used for IPCC AR5), have been achieved. In this study, we used CMIP5 outputs from the IAP coupled model to answer this question: What are the possible changes in EAWM in the future scenarios of RCP4.5 and RCP8.5 in terms of climatology and interannual variations? Section 2 of this paper contains a description of the IAP-coupled climate system model and the CMIP5 experimental designs. The datasets and methodology used in this study are given in section 3. In section 4, the results from the model's projections (RCP4.5 and RCP8.5) are presented. We analyzed the changes in EAWM basic modes and its associated general circulation pattern by the end of the 21st century. A brief discussion and conclusions are given in the last section.

2. Model and Experiment design

2.1 *Introduction of the IAP FGOALS model*

The IAP climate system model used in this study is the second spectral version of the Flexible Global Ocean–Atmosphere–Land System model (FGOALS2-s); this model has provided state-of-the-art computer simulations of the Earth's past, present, and future climate states (Zhou et al., 2005; Bao et al., 2010b). The atmospheric component is the Spectral Atmospheric Model of the IAP/LASG (SAMIL; horizontal resolution 2.81° longitude ×1.66° latitude with 26 hybrid vertical layers) (e.g., Wu et al., 1996; Wang et al., 2005; Bao et al., 2010b). The oceanic component is the LASG IAP Common Ocean Model (LICOM; grid resolution 1°×1°, with the increased resolution to 0.5°×0.5° in tropical regions; Liu et al., 2004). The other components, including land surface, ice, and coupler components, are from the NCAR CCSM (Kiehl and Gent, 2004).

2.2 *Introduction of the IPCC AR5 scenarios*

To investigate the projected changes in the EAWM, results from three groups of CMIP5-coordinated experiments with FGOALS2-s were used to perform historical simulations, RCP4.5 future projections, and RCP8.5 future projections. The historical simulations were integrated from 1850 to 2005; and both RCP4.5 and RCP8.5 were projected from 2006 to 2100. RCP4.5 indicates a concentration pathway that results in a radiative forcing of ∼4.5 W m^{-2} at year 2100, and RCP8.5 indicates a concentration pathway that results in a radiative forcing of ∼8.5 W m^{-2} at year 2100, relative to preindustrial conditions (i.e., the year 1850; Taylor et al., 2009). RCP4.5 is a stabilization scenario in which total radiative forcing is stabilized before 2100, without overshooting, using a range of new technologies and strategies for reducing greenhouse gas emissions (GHGs). RCP 8.5 is characterized by increasing GHGs over time, leading to higher GHG concentrations.

The changing conditions imposed on historical simulations and future projections include atmospheric composition (including CO_2) due to anthropogenic and volcanic influences, solar forcing, and concentrations of short-lived species and natural and anthropogenic aerosols. These experiments are all standard runs based on CMIP5 experimental design (Taylor et al., 2009; Moss et al., 2010). To reduce the uncertainties arising from differing initial conditions, historical simulations and RCPs projections have three ensemble members that were started from the different conditions of the preindustrial-scenario experiment. The following analyses were derived from these three ensemble means. For the interannual variability and basic modes studies, the analyses were performed for each member, and then the ensemble was completed for the three members.

3. Data and methodology

The datasets used to evaluate the model included the reanalysis circulation fields from the National Centers for Environmental Prediction-National Center for Atmospheric Research (NCEP-NCAR; Kalnay et al., 1996; Kistler et al., 2001): monthly mean temperature, geopotential height, and horizontal velocity. These data have a grid resolution of 2.5°×2.5°, and they extend from 1000 hPa to 10 hPa, with 17 vertical pressure levels. The reanalyzed surface air temperature (SAT) and meridional wind were also examined. To be consistent with the reanalysis datasets, all of the simulation results were converted to a grid resolution of 2.5°×2.5°.

Our analyses focused on the boreal winter. Therefore, the wintertime mean was computed by averaging 3-month periods [December–February (DJF)] in each year. Finally, the climatologic wintertime means were calculated by averaging each DJF over the period of model experiments. Correlation and regression studies were adopted in this study. We also used partial correlation and regression analyses to exclude the possible influence of one factor from that of another. The two-tailed Student's t-test was employed to test the significance of the results. If the individual 30 winters of data were independent of each other, the correlation coefficients corresponding to the 5% and 1% significance levels were 0.36 and 0.46, respectively.

To get the basic modes of EAWM interannual variability, EOF analysis was applied in this study; it was conducted by constructing an area-weighted covariance matrix. The wintertime (DJF) mean gridded data were weighted by the square root of cosine of latitude to ensure that equal areas were afforded equal weight in the analyses. We regressed the wintertime unweighted anomaly fields upon the standardized principal component (PC) time series and plotted the resulting regression coefficients. In this way, the values in the regression maps corresponded to anomaly values that were associated with one standard deviation anomalies in the PC time series.

In this study, AO index was defined as the zonal-averaged sea level pressure (SLP) anomalies between 35°N and 65°N (Li and Wang, 2003), which were highly correlated with AO index defined using EOF analysis by Thompson and Wallace (1998). However, the results of Li and Wang (2003) show a more pronounced annular ring structure than the EOF AO index. We also used the stratospheric polar-night jet index, which was defined using the zonal-mean wind at 60°N at the middle stratosphere (30 hPa), an index measuring the strength of the circumpolar wind, and the strength of the polar vortex in the stratosphere.

4. Results

4.1 *The climatology*

The EAWM is characterized by strong zonal (west–east) pressure gradient between the Siberian High and the Aleutian Low, which are highly associated with the stationary planetary-scale asymmetric forcing, i.e., the topographic and diabatic heating features arising from the distribution of land and oceans (Lau and Chang, 1987; Chan and Li, 2004). The EAWM is also characterized by the strong surface northerly and deep longwave trough along the EA coastal region (Chen and Graf, 1998; Chen and Sun, 1999). Therefore, the main feature of the EAWM can be described by the surface zonal pressure contrast, the northerly at the lower level, and the tough state at the middle levels.

Before showing the projected changes of the EAWM, the general performance of FGOALS2-s is presented by comparing the historical simulations and observations. In Fig. 1, we showed the observational, historical simulated, and projected EAWM climatology, with the vectors representing the lower level wind (850 hPa), the shadings for SLP, and the contours for the 500-hPa geopotential height. We also examined in several key parameters (Table 1) that are usually used as the strength or state of the EAWM. These parameters include the following:

(1) $I_{\rm SH}$, the Siberian High index (Wu and Wang, 2002), SLP averaged for the domain: 40°–60°N, 80°–120°E.

(2) $I_{\rm SLPEC}$, the SLP averaged for the eastern China domain: 25°–40°N, 110°–120°E.

(3) $I_{\rm v}$, the low-level northerly index along the EA coastal region (Chen and Sun, 1999), the 1000 hPa northerly averaged for the domain: 15°–30°N, 115°–130°E.

(4) $I_{\rm wind}$, the regional wind velocity index at 850 hPa (Wang et al., 2004), 850-hPa wind speed averaged for the domain: 25°–50°N, 115°–145°E.

(5) $I_{\rm trough}$, the 500-hPa trough index (Cui and Sun, 1999), 500-hPa geopotential height averaged for the domain: 35°–40°N, 110°–130°E.

(6) $I_{\rm jet}$, the 200-hPa East Asian jet strength index (Yang et al., 2002), 200-hPa zonal wind averaged for the domain: 30°–35°N, 130°–160°E.

As illustrated in Fig. 1a (NCEP reanalysis) and Fig. 1b (historical simulation), the FGOALS2-s model captured clear EAWM features, such as the zonal pressure contrast between the Siberian High and the Aleutian Low, the broad trough along coastal East Asia, and the northerly at the mid-latitudes. The influence of the Tibetan Plateau was also very clear, with strong circum-Plateau flow at both the north and south sides of the Plateau, and the southward extension of the

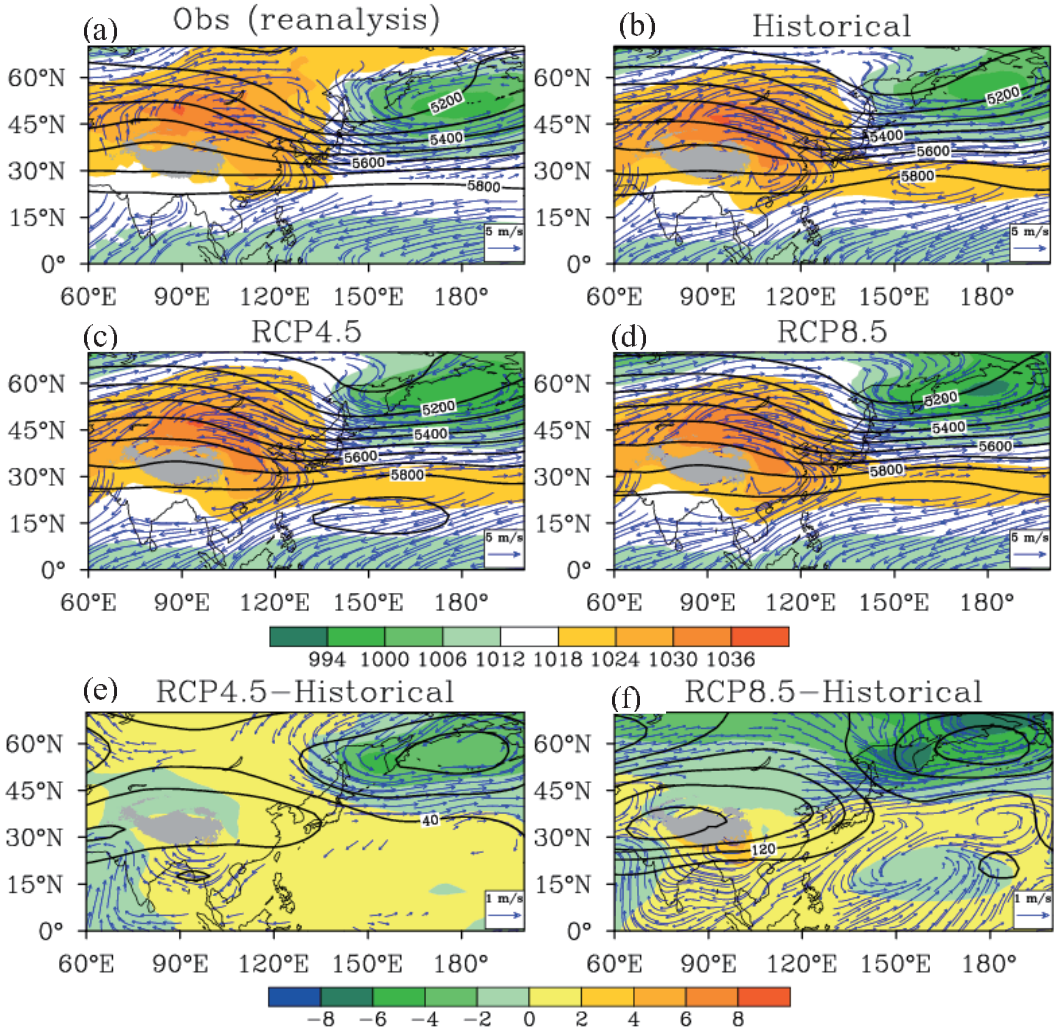

Fig. 1. The mean state of DJF sea level pressure (color shading, units: hPa), the 500-hPa geopotential height (contours, units: gpm) and 850-hPa wind vector (vector, units: m s^{-1}). (a) Observation, NCEP/NCAR reanalysis data (30-year climatology from 1971 to 2000), (b) CMIP5-historical, the historical model simulation (averaged from 1971 to 2000), (c) CMIPS-RCP4.5 (2071–2100), (d) CMIPS-RCP8.5 (2071–2100), (e) the differences between RCP4.5 and historical runs, (f) the differences between RCP8.5 and historical runs.

Siberian High downstream of the Tibetan Plateau over eastern China. The position of the center of the Siberian High (around the region 40°–60°N, 80°–120°E) was very well set in the historical simulation, as it was in the observation (Wu and Wang, 2002). The intensity of the Siberian High was also precisely simulated (refers to the I_{SH} in Table 1). However, the southward extension of the Siberian High downstream of the Tibetan Plateau over eastern China was somewhat stronger in the historical simulation than in the NCEP reanalysis. The average SLP was 1028.5 hPa over the eastern China (25°–40°N, 110°–120°E) in the historical simulation, compared with 1025.7 hPa in the NCEP reanalysis.

Although the model simulated a good and reasonable wind distribution, its wind speed was stronger than that shown in the observation at higher and lower latitudes. In the mid-latitudes along East China, there was stronger northerly wind in the model, probably associated with the stronger SLP over this region. The low-level northerly wind index, I_v, was 4.8 m s^{-1} in the historical run, in comparison with the 4.6 m s^{-1} in the NCEP reanalysis, which is also confirmed by the 850-hPa wind velocity index, I_{wind}, with 6.5 m s^{-1} in reanalysis and 6.6 m s^{-1} in the historical run. The strength of the Aleutian Low was somewhat underestimated compared with the observation (see I_{AL} in Table 1), and its position shifted slightly north of that

Table 1. The statistics of the EAWM parameters.

	a. $I_{\rm SH}$	b. $I_{\rm SLPEC}$	c. $I_{\rm v}$	d. $I_{\rm wind}$	e. $I_{\rm trough}$	f. $I_{\rm jet}$
NCEP-reanalysis	1029	1025.7	−4.6	6.5	5492	66.1
CMIP5-historical	1029	1028.5	−4.8	6.6	5507	53.7
CMIPS-RCP4.5	1029	1028.9	−4.9	6.8	5561	55.0
CMIPS-RCP8.5	1028	1029.0	−5.4	7.1	5638	56.5

a. $I_{\rm SH}$, the Siberian High index (Wu and Wang, 2002), SLP averaged for the domain: 40°–60°N, 80°–120°E.

b. $I_{\rm SLPEC}$, the SLP averaged for the eastern China, the domain: 25°–40°N, 110°–120°E.

c. $I_{\rm v}$, the low-level northerly index along the East Asian coastal region (Chen and Sun, 1999), the DJF northerly at 1000 hPa averaged for the domain: 15°–30°N, 115°–130°E.

d. $I_{\rm wind}$, the regional wind velocity index at 850 hPa (Wang and Jiang, 2004), 850-hPa wind speed averaged for the domain: 25°–50°N, 115°–145°E.

e. $I_{\rm trough}$, the 500-hPa trough index as in Cui and Sun (Cui and Sun, 1999), 500-hPa geopotential height averaged for the domain: 35°–40°N, 110°–130°E.

f. $I_{\rm jet}$, the 200-hPa East Asian jet strength index (Yang et al., 2002), 200-hPa zonal wind averaged for the domain: 30°–35°N, 130°–160°E.

in the NCEP reanalysis. The model showed a weaker trough at the mid-levels and weaker jet strength at the upper level, indicating a weaker baroclinicity at the mid-latitudes in the model. The EAWM trough index was 5507 gpm in the historical run, while it was only 5492 gpm in the NCEP reanalysis, which caused a westward shift of the EAWM major trough. The simulated 200 hPa jet index was 53.7 m s^{-1}, much weaker than the observational value of 66.1 m s^{-1} in the reanalysis.

Figures 1e and f display the differences between RCP4.5/RCP8.5 projections and historical simulations, which exhibit the projected changes of climatological EAWM. The low-level wind around the eastern and southern coastal regions intensified (Figs. 1c–f), especially the northwesterly over the northeastern Asia and the easterly over the Indo-China Peninsula. The averaged wind velocity over northeastern Asia (40°–50°N, 130°–140°E) increased 10% for the RCP4.5 and 16% for the RCP8.5 projections, respectively. And the averaged wind velocity over the Indo-China Peninsula (the domain: 10°–20°N, 80°–110°E) increased 8% and 12% for the RCP4.5 and RCP8.5 projections, respectively. Over eastern China, the low-level northerly wind index, $I_{\rm v}$, increased in the RCP4.5 and RCP8.5 projections. Particularly in the RCP8.5 projection, the northerly wind $I_{\rm v}$ exhibited an 11% increase, and the 850 hPa wind index $I_{\rm wind}$ also exhibited an 8% increase (Table 1).

4.2 *The seasonal cycle* (*winter monsoon*)

The annual cycle of temperature over the EA regions (averaged from 110°E to 120°E) is displayed in Fig. 2. The winter season evolution is featured with temperature dropping in late autumn and early winter, and temperature rising in late winter and spring. This seasonality is synchronous with the seasonal march and retreat of the EAWM. Compared with the temperature seasonal evolution derived from NCEP reanalysis, FGOALS2-s reasonably captured the cold period and its southward extension in historical simulations (Figs. 2a and b). At 40°N, the average temperature dropped below 0°C in mid-November, declined to minimum in January, and rose above 0°C in early February. The 0°C line extended to ∼34°N in January. These features are consistent with the observation data, while the exact winter time was shorter. Table 2 shows the starting date, ending date, and duration of the time that the average temperature remained below 0°C at 40°N. The simulated winter started ∼1 week later and ended ∼10 days earlier.

Under the RCP4.5 scenario with moderate anthropogenic forcing and global warming, the EA regions warmed ∼2°C in the winter season. North China (∼40°N) underwent warming of ∼4°C (Figs. 2c and e). The cold season period shortened. At 40°N, the aver-

Table 2. The starting date, ending date and duration of the time that the average temperature stays below 0°C at 40°N.

	NCEP	Historical	RCP4.5	RCP8.5
Starting date	13 Nov	19 Nov	26 Nov	15 Dec
Ending date	13 Mar	04 Mar	26 Feb	07 Feb
Duration (days)	122	105	92	54

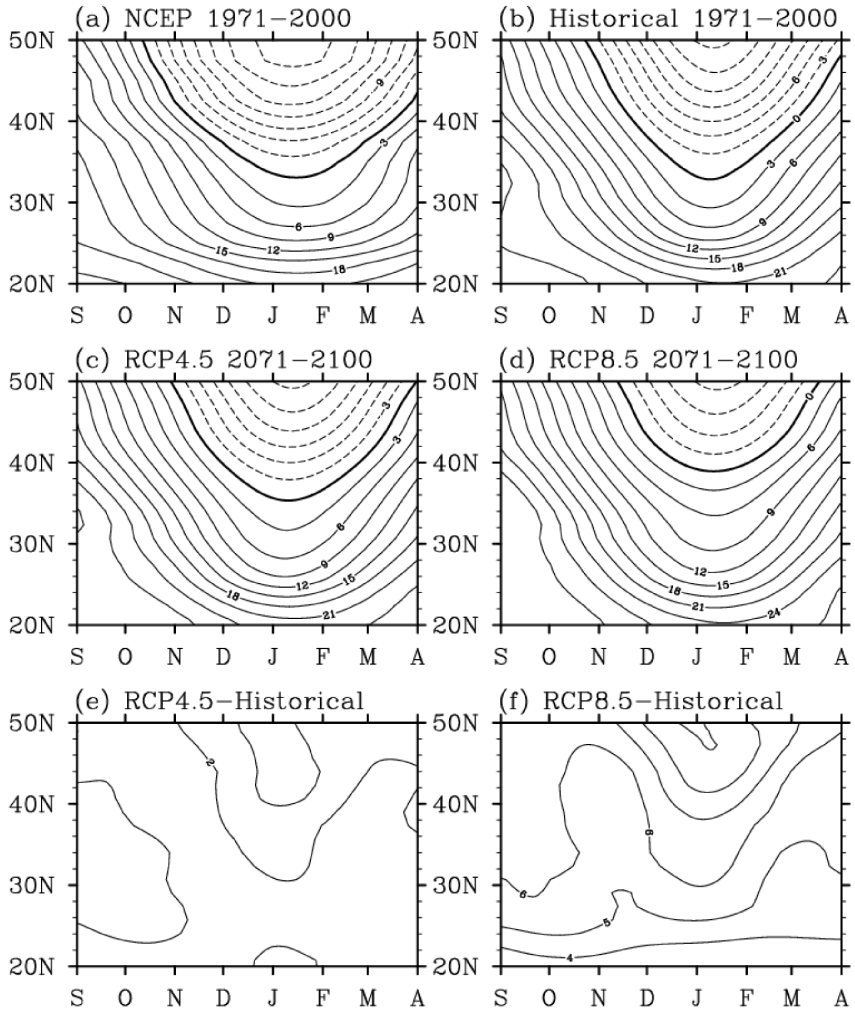

Fig. 2. Climatological annual cycle of 110°–120°E zonal-mean temperature in (a) NCEP reanalysis (averaged from 1971 to 2000), (b) CMIP5-historical (averaged from 1971 to 2000), (c) CMIPS-RCP4.5 (2071–2100), (d) CMIPS-RCP8.5 (2071–2100), (e) the differences between RCP4.5 and Historical runs, (f) the differences between RCP8.5 and historical runs.

age temperature dropped below 0°C in late November and rose above 0°C in late February. The 0°C margins withdrew to ∼36°N in January. The winter setup was postponed for ∼1 week, and winter withdrawal was earlier by ∼1 week, which caused the wintertime to be 2 weeks shorter than that of the historical run. Under the RCP8.5 scenario with the strong anthropogenic forcing and global warming, the EA regions warmed ∼3.5°C at 20°N, ∼6°C at 30°N, ∼7°C at 40°N in the winter season. The warming was greater in the winter than in other seasons. The cold season period was greatly compressed. At 40°N, the average temperature dropped below 0°C in mid-December and rose above 0°C in early February. The 0°C range retreated to ∼40°N in January. The winter setup was postponed for ∼1 month, and the winter withdrawal was brought earlier by ∼1 month, which together caused the winter time to be ∼50 days shorter than in the historical run.

Although a remarkable warming trend occurred in East Asia, the prevailing northerly wind increased under the global warming RCP4.5 and RCP8.5 scenarios. The projected monthly northerly wind is shown in Fig. 3. The historical run reproduced the northerly wind seasonal evolution and its amplitude in the cold season: northerly wind increased in late autumn and early winter and peaks emerged in mid-winter (December and January) and decreased in late winter and early spring. The model simulated a postponed winter season setup and earlier winter season ending, as manifested by the southerly in September and April, compared with the weak northerly from the observation data. The southerly increased in RCP4.5 and RCP8.5

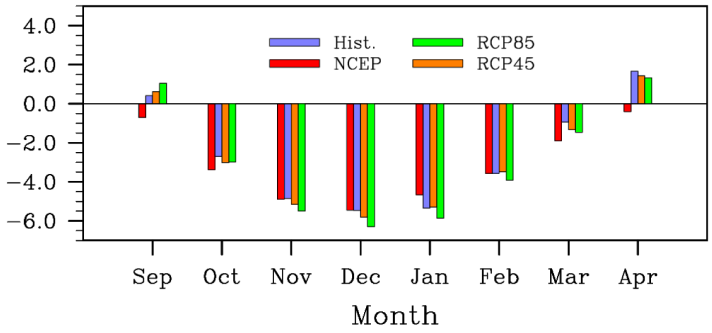

Fig. 3. The monthly low-level northerly index along the East Asian coastal region (averaged for the region: 15°–30°N, 115°–130°E at 1000 hPa).

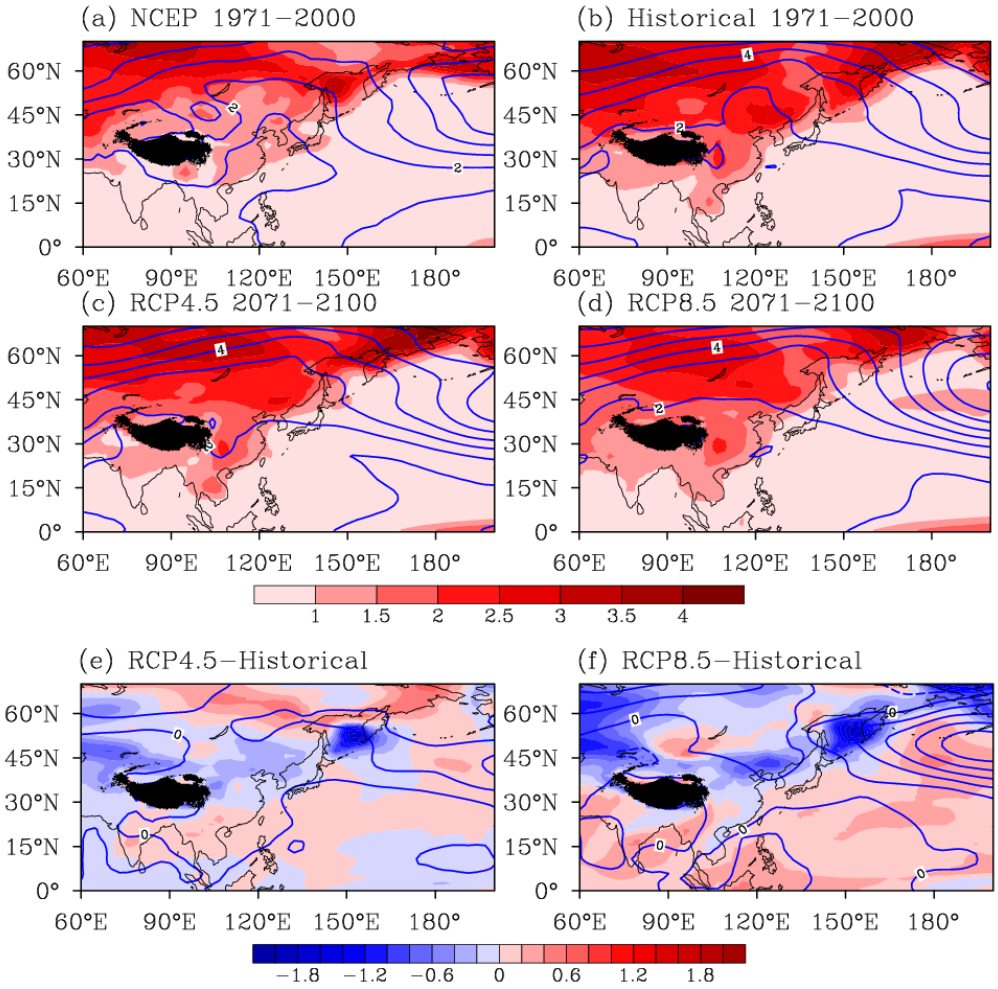

Fig. 4. The standard deviation (STD) of the surface air temperature (shading) and the sea level pressure (contours). (a) Observation, NCEP/NCAR reanalysis data (30-year climatology from 1971 to 2000), (b) CMIP5-historical, the historical model simulation (averaged from 1971 to 2000), (c) CMIPS-RCP4.5 (2071–2100), (d) CMIPS-RCP8.5 (2071–2100), (e) the differences between RCP4.5 and historical runs, (f) the differences between RCP8.5 and historical runs.

projections in September and April, indicating the compressions of winter season at the both ends. The northerly increased in the RCP4.5 projection in October, November, and December (mainly the early winter), while it increased in almost all the winter months (from November through March) in the RCP8.5 projection. The increase of northerly wind in the cold season suggests that the strength of the EAWM might increase in spite of the general warming.

4.3 *The interannual variability*

The intensity of interannual variability of the EAWM can be described with the standard deviation (STD) of the winter monsoon parameter. In Fig. 4, the plots of the STD of the surface temperature (shading) and the SLP (contour) are shown. The STD of surface temperature is largest at high latitudes. Substantial variability also occurred over eastern China, presenting as a significant southward extension over this region. The historical simulation reproduced the large variability at high latitudes, and the southward extension over eastern China. In the RCP4.5 and RCP8.5 projections, the STD increased south of the Siberian High, over South Asia, Southeast Asia, and the North Pacific, while STD decreased west of the Siberian High, over northern China, and around northern Japan.

The ratio of STD between the scenario projections and the historical run were plotted (Fig. 5) for the EA regions (averaged from 110°E to 120°E); the solid line indicates the RCP4.5 projection and the dashed line indicates the RCP8.5 projection. The STD decreased over most of eastern China, with the largest decrease around 40°N. The ratio was ∼0.85 in RCP4.5 and ∼0.7 in RCP8.5 around 40°N. Because large temperature variation is usually associated with strong cold surge activity, a decrease of the temperature STD suggests that the EAWM will be stable and the hazards caused by cold surges will be relieved over eastern China. The STD over the South China Sea, however, increased in RCP4.5 and RCP8.5, especially in RCP8.5. This strong increase of the STD indicates stronger cold surge activities over this region, consistent with the stronger northerly winds discussed in the previous section.

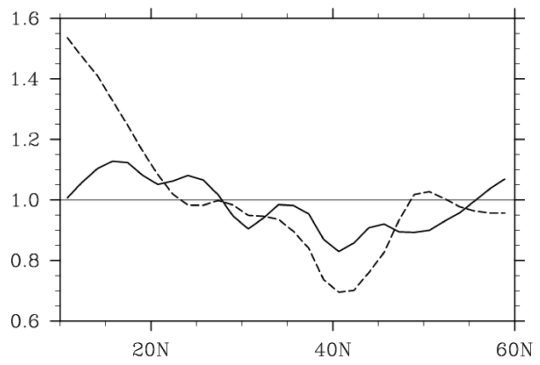

Fig. 5. The radio of the standard deviation of the 110°–120°E zonal-mean temperature between the CMIPS-RCP4.5 and the CMIP5-historical (the solid line), and between the CMIPS-RCP8.5 and the CMIP5-historical (the dashed line).

4.4 *The basic modes of the EAWM*

Figure 6 shows the observational, simulated, and two projected leading patterns of the EAWM, which were derived by performing EOF analyses of the surface air temperature (SAT) over the EAWM domain (0°–60°N, 100°–140°E) as in the work of Wang et al. (2010). We regressed the DJF mean low-level (925-hPa) wind, SAT, and SLP upon the standardized principal component (PC) time series and examined the resulting regression coefficients. As in the work of Wang et al. (2010), the first two distinct modes dominated most of the total temperature variance: the first mode showed the largest variance in the northern EA and decreased southward, and the second mode featured a seesaw pattern between the northern EA and the southern EA (Figs. 6a and b). These two modes were associated with notably different circulation structures and sources of variability, like those of Wang et al. (2010). Whereas Wang et al. (2010) focused on predictability and attributed the WAWM basic modes to external forcing (i.e., the preceding snow covers over southern Siberia–Mongolia and ENSO events), we analyzed the crucial atmospheric internal modes.

The first EAWM mode was highly correlated with AO. The correlation coefficient (CC) between the PC1 and the AO index was 0.78 during the period 1971–2000, above the 99% confidence level. When AO was in a positive phase, all of East Asia, especially the northern region, tended to be warmer than normal. Likewise, when AO was in a negative phase, northern East Asia tended to be colder than usual. The second EAWM mode, however, was highly correlated with the strength of the stratospheric polar vortex. The CC between PC2 and the stratospheric polar jet index (the zonal-mean zonal wind at 65°N, 30 hPa) was 0.57 when NCEP reanalysis data was used. Considering the high correlation between AO and the jet index (CC = 0.47), the partial correlation coefficient (pCC) was calculated to exclude the influence from the other. The pCC between PC1 and AO was 0.76, and the pCC was 0.61 between PC2 and the jet stream index, which was still highly significant.

We further analyzed the relations among the EAWM, AO, and the stratospheric polar vortex

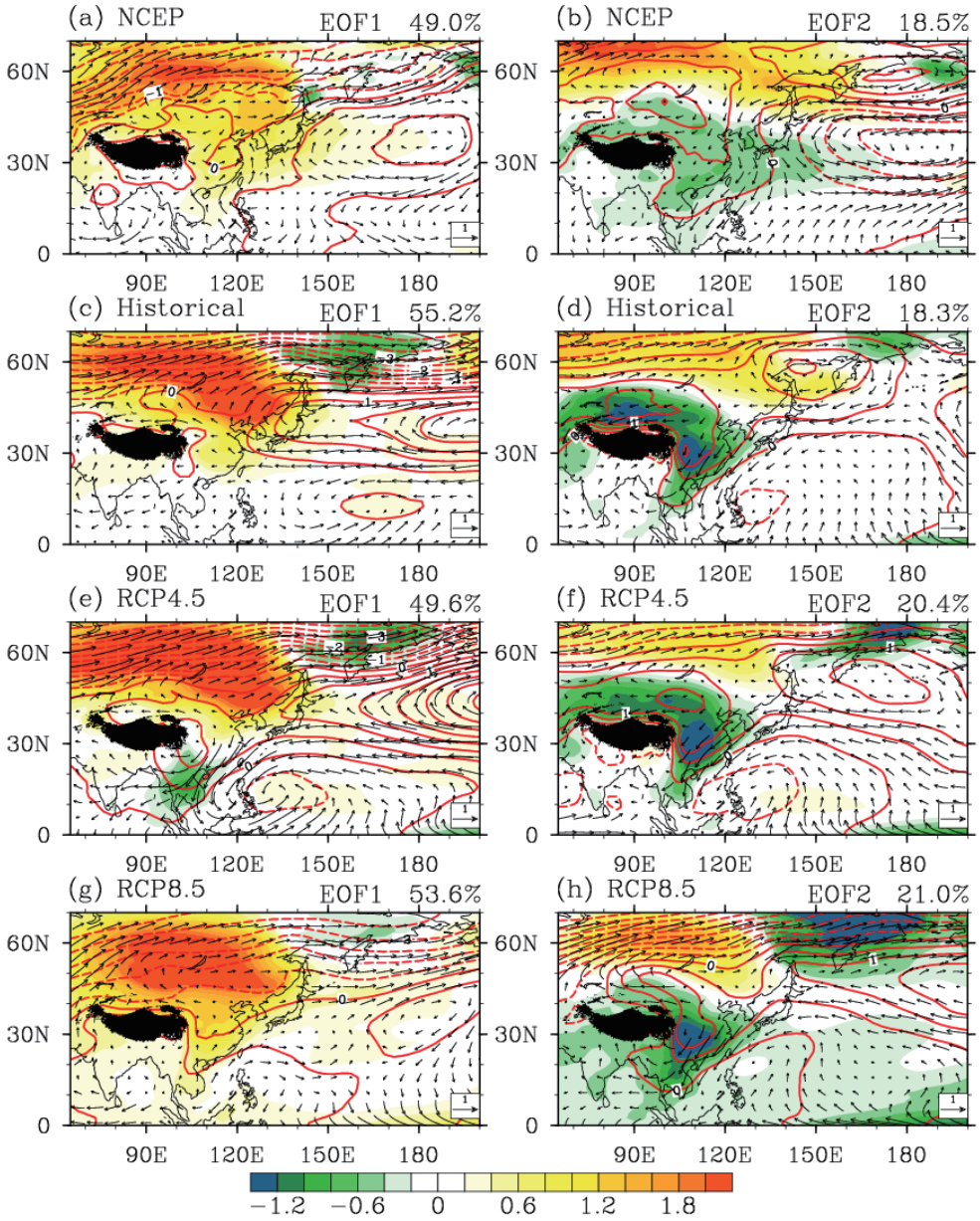

Fig. 6. The spatial patterns of the first two EOF modes of surface temperature over the domain: 0°–60°N, 100°–120°E. All panels are 925 hPa winds (vectors, units: m s^{-1}), surface temperature (color shading, units: °C), and sea-level pressure (contours, units: hPa). From upper to bottom: Observations based on NCEP reanalysis (a–b), CMIP5-Historical (c–d), CMIP5-RCP4.5 (e–f), and CMIP5-RCP8.5 (g–h).

strength (Fig. 7); theses analyses reveal a partial regression pattern of circulation variables over East Asia with AO and stratospheric jet index. The partial regression (Fig. 7a) between the EAWM and AO is almost identical to the regression pattern of EAWM leading mode (Fig. 6a) in NCEP reanalysis, with warming over Asian continent in association with a positive AO. The warming was biased toward the high latitudes, accompanied by westerly anomalies in this region. Positive SLP anomalies occurred over the mid-latitudes of the northern Pacific, leading to the southerly anomalies to the west of the positive SLP center near the EA coastal region. The partial regression between EAWM and stratospheric jet strength was characterized by temperature cooling and northerly anomalies over East Asia, with largest ampli-

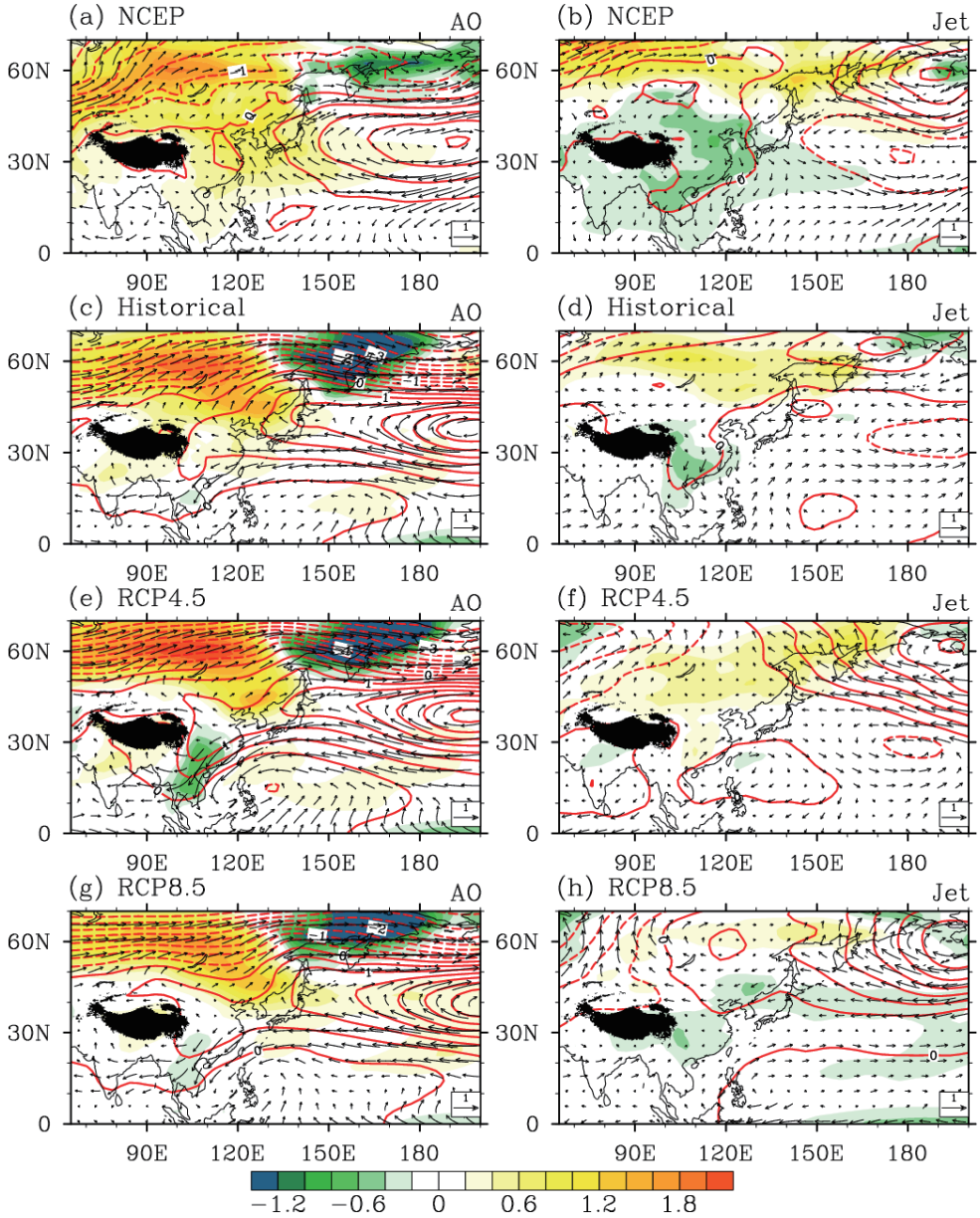

Fig. 7. The partial regression patterns of the surface temperature (color shading, units: °C), sea-level pressure (contour, units: hPa) and 925-hPa winds (vectors, units: m s^{-1}) with AO (left column) and stratospheric jet strength (right column). From upper to lower panels: Observations based on NCEP reanalysis (a–b), CMIP5-Historical (c–d), CMIP5-RCP4.5 (e–f), and CMIP5-RCP8.5 (g–h).

tude over southern China, which was similar to the regression pattern of the second EAWM mode (Fig. 6b), also called the southern mode by Wang et al. (2010).

In the historical simulation, the model captured the two leading modes very well (Figs. 6c and d). However, the warming center in EOF1 extended southward to Northeast China, and the anticyclone over middle northern Pacific and the cyclone over the subtropical northern Pacific both extended westward. The cooling over southern China in EOF2 increased, while the warming over higher latitudes decreased, and the anticyclone over the Bering Sea moved over the Okhotsk Sea. The leading mode was highly correlated with AO, illustrated by a high CC of 0.69, and a pCC of 0.61. The AO regression (Fig. 7c) showed the largest warming anomalies in northern East Asia, positive SLP anomalies over the middle northern Pacific, and circumpolar westerly over higher latitudes, similar to

Table 3. Correlation coefficients between the two leading PCs and Arctic Oscillation (AO) index and stratospheric polar jet index in observations, CMIP5-historical, CMIP5-RCP4.5, CMIP5-RCP8.5. The numbers in the brackets are the pCCs between leading PCs and AO (jet) index, excluding the influence of the jet (AO) index. The numbers with ** and * indicate the value above the 99% and 95% statistical confidence level, respectively.

	AO				Polar Jet			
	NCEP	Hist	RCP45	RCP85	NCEP	Hist	RCP45	RCP85
PC1	0.78**	0.69**	0.78**	0.51**	0.30	0.45*	0.62**	0.29
	(0.76**)	(0.61**)	(0.60**)	(0.45*)	(−0.13)	(0.11)	(0.23)	(−0.10)
PC2	0.08	0.28	0.30	0.58**	0.57**	0.40*	0.13	0.54**
	(−0.27)	(0.04)	(0.29)	(0.36)	(0.61**)	(0.31)	(−0.10)	(0.26)

the observation data (Fig. 7a) and the EAWM leading mode (Fig. 6a). The PC1 was correlated with the strength of stratospheric polar vortex with a CC of 0.45; while the pCC between them was only 0.11 after excluding the high correlation between AO and the stratospheric polar vortex (CC=0.56). The second mode was correlated with the stratospheric jet index with a CC of 0.40 and a pCC of 0.31; therefore, this model is capable of reproducing the stratosphere–EAWM relationship in spite of its coarse resolution in the stratosphere. The jet index regression pattern also occurred in the historical simulation (Fig. 7d): cooling occurred over southern East Asia, and the SLP seesaw pattern emerged between the middle and higher latitudes over the northern Pacific. However, their amplitudes were much weaker than those derived from the NCEP reanalysis.

In the RCP4.5 projection, the AO influence (Fig. 7e) intensified in the lower latitude, illustrated by the strong cyclone center over the Philippines and the South China Sea, suggesting a stronger AO–tropics interaction under the RCP4.5 scenario. The strong cyclone caused strong northerly winds over southern China, leading to the cooling center there. The PC1 was highly correlated with AO (CC=0.78, pCC=0.61). Although the correlation between PC1 and the stratospheric jet index was significant (CC=0.62), the pCC was only 0.22 after removing the high correlation between AO and stratospheric jet index (CC=0.65). Therefore, the leading EAWM mode was mainly contributed by AO, which can be confirmed by the regression map of AO (Fig. 7e). The northern center of the EOF2 mode, however, decreased in amplitude, protruding the importance of the southern center over southern China and Indo-China Peninsula. This mode was highly associated with a cyclonic anomaly over northwest Pacific, mainly in associated with AO as shown in Fig. 7e.

The warming in the EAWM leading mode was concentrated over Siberia under the strong warming forcing of the RCP8.5 scenario. The amplitudes of the circulation anomalies over northern Pacific decreased. The leading mode was highly correlated with AO (CC=0.51, pCC=0.45). The second mode, however, was highly correlated with AO and the stratospheric jet index. The correlation coefficients were 0.58 and 0.54, respectively, indicating the combined influences of large-scale atmospheric circulation anomalies on the local climate from both the lower troposphere and the stratosphere. Figures 7g and h show that the temperature anomalies over northern EA were mainly attributable to the influence of AO, while temperature anomalies over southern EA were partly influenced by the strength of the stratospheric polar vortex.

Comparing historical simulations and RCP projections, the total variation explained by the second EAWM EOF mode distinctly increased from 18.3% to 21%. This increase indicates that the second EAWM mode became more dominant in the future projections. As shown in Table 3, the pCCs between PC1 and AO in the projections decreased from historical simulations to future projections, indicating that the relationship between the EAWM leading mode and AO weakened. Meanwhile, the CCs between PC2 and AO in projections increased from historical simulations to future projections. The CCs between AO and the stratospheric jet index were 0.56 in the historical run, 0.65 in the RCP4.5 scenario, and 0.67 in the RCP8.5 simulation, indicating the possibility of a stronger coupling between the troposphere and stratosphere in the projections. However, AO can vary spatially. For example, shape changing, area shrinking, and extending and boundary swinging can occur (Zhao et al., 2010). The influence pattern of AO can be modulated by future global warming, increasing the complexity of the predictability of EAWM interannual variations.

5. Discussions and conclusions

We studied the projected change of EAWM basing on the CMIP5 coordinated experiments with IAP coupled model FGOALS2-s. The changes of climatology, seasonality, and interannual variations have been respectively reported. Based on historical simulations

and RCP4.5/RCP8.5 projections, the projected results indicate strong warming, especially in the winter season. The warming increased with latitudes, ranging from 1°C to 3°C in the RCP4.5 scenario and from 4°C to 9°C in the RCP8.5 projection. The northerly wind over the coastal region of East Asia, became stronger in the two scenarios, indicating a stronger EAWM. This result differs from some previous simulations (e.g., Hu et al., 2000; Bueh, 2003; Jiang et al., 2010). For example, using 19 IPCC AR4 climate models with A2, A1B and B1 scenarios, Jiang et al. (2010) projected that the winter wind speeds decreased in China for the 21st century due to a weakened EAWM.

The stronger winds in this study are associated with two systems in the simulation: the deeper low over the polar cap, and the much deeper low in the high latitudes of the North Pacific. Several studies have reported a positive AO trend as the response to anthropogenic GHG forcing (e.g., Fyfe et al., 1999; Yamaguchi and Noda, 2006; Hori et al., 2007; Zhu and Wang, 2010). The AO indices in our study were 15.6 in the historical simulation, 16.3 in the RCP4.5 projection, and 18.5 in the RCP8.5 projection. Therefore, our model estimated an increase of AO under the global warming background, in accord with previous studies. This deepened the polar low and strengthened the circumpolar westerly.

On the other hand, many studies have reported an ENSO-like SST change under the global warming background (e.g., Meehl and Washington, 1996; Knutson et al., 1998; Cai and Whetton, 2001; Yamaguchi and Noda, 2006; Kug et al., 2011). For example, Yamaguchi and Noda (2006) simulated an ENSO-like global warming pattern in the tropics by the majority of the 18 IPCC AR4 model results. Kug et al. (2011) further discussed the possible mechanism for the El Niño-like warming in response to the greenhouse warming. It is well known that El Niño is associated with strong negative SLP anomalies in the high latitudes of the North Pacific, i.e., the stronger Aleutian Low (Yamaguchi and Noda, 2006). Therefore, we considered the deeper Low in the high latitude of north Pacific to be associated with the El Niño-like SST pattern, which resulted from the anthropogenic GHG forcing. Notably, the winter monsoon is caused by the asymmetry of topographic and diabatic forcing associated with the distribution of land and oceans (Lau and Chang, 1987; Chan and Li, 2004). Therefore, the relation between the global-scale homogenized warming and regional asymmetry EAWM requires further study.

The increase of the winds along the East Asian coastal region might have some influence on the following Asian summer monsoon. As Yan et al. (2011) pointed out, the EAWM persistently impacts the variation of SSTs in the tropical Indian Ocean and the South China Sea, and a strong EAWM leads to a strong EASM in the following summer. Therefore, the atmosphere–ocean interaction in the tropical Indian Ocean and the South China Sea will probably be more important and lead to stronger EASMs under the warming scenarios.

The interannual temperature variability decreased over eastern China, especially North China, which implies a less disturbed EAWM and the relief of hazards caused by cold surges. However, the temperature variability increased around the South China Sea and lower latitudes in the 21st century under the RCP4.5 and RCP8.5 scenarios, especially under the latter, which indicates active EAWM and more cold surges. The greater response of temperature variability to RCP8.5 than to RCP4.5 implies that variability may be intensified along with the extent of increases in GHGs, which will have greater impacts on society and the economy.

The interannual variation of the EAWM was dominated by two modes; the leading mode featured a northern mode, and the second featured a southern mode. We found that these two modes were associated with AO and the strength of the stratospheric polar vortex, respectively. Due to the high correlation between low-level AO and the strength of stratospheric polar vortex, the influences from these two circulation components are usually mixed. Until now, few studies have distinguished their individual roles. Further studies are needed to investigate the influence of stratospheric polar vortex on the EAWM and its the mechanisms, and to discriminate it from AO.

The future projections of two levels of expected radiative forcing, RCP4.5 and RCP 8.5 were conducted The second EAWM EOF pattern featured a seesaw pattern in temperature between southern and northern EA, which explains more total variance in the warmer projection RCP8.5, suggesting more influence from the variation of stratospheric polar vortex. The partial correlation between AO and PC1 decreased from the historical simulation to the future projections, while the correlation between AO and PC2 increased, indicating the possibility of stronger coupling between the troposphere and stratosphere in the future. This changing relationship complicates the connection between EAWM and AO and adds complexity to the predictability of EAWM interannual variations.

Although internal processes are important in the variation of EAWM, the EAWM can also be influenced by external forcing, such as ENSO (e.g., Li, 1990; Zhang et al., 1996; Feng et al., 2010), SST over the tropical western Pacific warm pool (Huang and

Sun, 1992; Chen et al., 2000), the thermal states of the Tibetan Plateau (Ye ang Gao, 1979), and Eurasian snow cover (Wu and Zhang, 1998; Jhun and Lee, 2004). Wang et al. (2010) pointed out that only the second EAWM mode can be affected by ENSO and that the first EAWM mode is possibly ENSO independent on the interannual time scale. Zhou et al. (2007a, b) found that the EAWM–ENSO relationship might have interdecadal variation, and that EAWM has connection with the SST interdecadal variability over the Eastern North Pacific on decadal time scales. Therefore, further attention should be given to the EAWM–SSTA interaction using the state-of-the-art AR5 coupled models under the new scenarios.

Our results should be used with caution because they are derived from a single model, despite the ensemble technique. Presently, multi-model ensemble results are generally used for climate-change evaluation and projection (e.g., IPCC AR4 and its precursors). Multi-model results can avoid model biases from each single model and thereby reduce the projected uncertainties. Therefore, AR5 runs from other model centers should be used to create an ensemble with greater model reliability.

Acknowledgements. This research is supported by the National Basic Research Program of China (973 Program) (Grant Nos. 2010CB428603 and 2012CB417203), and the National Natural Science Foundation of China (Grant No. 41175041).

REFERENCES

Bao, Q., J. Yang, Y. Liu, G. Wu, and B. Wang, 2010a: Roles of Anomalous Tibetan Plateau Warming on the Severe 2008 Winter Storm in Central-Southern China. *Mon. Wea. Rev.*, **138**, 2375–2384.

Bao, Q., G. Wu, Y. Liu, J. Yang, Z. Wang, and T. Zhou, 2010b: An introduction to the coupled model FGOALS1.1-s and its performance in East Asia. *Adv. Atmos. Sci.*, **27**, 1131–1142. doi: 10.1007/s00376-010-9177-1.

Bueh, C., 2003: Simulation of the future change of East Asian monsoon climate using the IPCC SRES A2 and B2 scenarios. *Chinese Science Bulletin*, **48**, 1024–1030.

Bueh, C., and L. Ji, 1999: Anomalous activity of East Asian winter monsoon and the tropical Pacific SSTA. *Chinese Science Bulletin*, **44**, 890–898.

Cai, W. J., and P. H. Whetton, 2001: A time-varying greenhouse warming pattern and the tropical-extratropical circulation linkage in the Pacific Ocean. *J. Climate*, **14**, 3337–3355.

Chan, J., and C. Y. Li, 2004: The East Asian winter monsoon. *East Asian Monsoon*, C.-P. Chang, Ed., World Scientific Publishing Company, 54–106.

Chang, C. P., J. E. Erickson, and K. M. Lau, 1979: Northeasterly cold surges and near-equatorial disturbances over the winter MONEX area during December 1974. I— Synoptic aspects. *Mon. Wea. Rev.*, **107**, 812–829.

Chen, J., and S. Q. Sun, 1999: East Asian winter monsoon anomaly and variation of global circulation. Part I: A comparison study on strong and weak winter monsoon. *Chinese J. Atmos. Sci.*, **23**, 101–111. (in Chinese)

Chen, W., and H. F. Graf, 1998: The interannual variability of East Asian winter monsoon and its relationship to global circulation. *Max-Planck-Institute for Meteorologic Report*, **250**, 1–35.

Chen, W., H. F. Graf, and R. Huang, 2000: The interannual variability of East Asian winter monsoon and its relation to the summer monsoon. *Adv. Atmos. Sci*, **17**, 46–60.

Cohen, J., K. Saito, and D. Entekhabi, 2001: The role of the Siberian high in Northern Hemisphere climate variability. *Geophys. Res. Lett.*, **28**, 299–302.

Cui, X., and Z. Sun, 1999: East Asian winter monsoon index and its variation analysis. *Journal of Nanjing Institute of Meteorology*, **22**, 321–325. (in Chinese)

Feng, J., L. Wang, W. Chen, S. K. Fong, and K. C. Leong, 2010: Different impacts of two types of Pacific Ocean warming on Southeast Asian rainfall during boreal winter. *J. Geophys. Res.*, **115**, D24122, doi: 24110.21029/22010JD014761.

Fyfe, J. C., G. J. Boer, and G. M. Flato, 1999: The Arctic and Antarctic oscillations and their projected changes under global warming. *Geophys. Res. Lett.*, **26**, 1601–1604.

Gu, L., K. Wei, and R. Huang, 2008: Severe disaster of blizzard, freezing rain and low temperature in January 2008 in China and its association with the anomalies of East Asian monsoon system. *Climatic and Environmental Research*, **13**, 405–418. (in Chinese)

Hori, M. E., D. Nohara, and H. L. Tanaka, 2007: Influence of Arctic Oscillation towards the Northern Hemisphere surface temperature variability under the global warming scenario. *J. Meteor. Soc. Japan*, **85**, 847–859.

Hu, Z. Z., L. Bengtsson, and K. Arpe, 2000: Impact of global warming on the Asian winter monsoon in a coupled GCM. *J. Geophys. Res.*, **105**, 4607–4624.

Huang, R., W. Chen, B. Yan, and R. Zhang, 2004: Recent advances in studies of the interaction between the East Asian winter and summer monsoons and ENSO cycle. *Adv. Atmos. Sci.*, **21**, 407–424.

Huang, R. H., and F. Y. Sun, 1992: Impacts of the Tropical Western Pacific on the East-Asian Summer Monsoon. *J. Meteor. Soc. Japan*, **70**, 243–256.

Jhun, J. G., and E. J. Lee, 2004: A new East Asian winter monsoon index and associated characteristics of the winter monsoon. *J. Climate*, **17**, 711–726.

Jiang, Y., Y. Luo, and Z. Zhao, 2010: Projection of wind speed changes in China in the 21st century by cli-

mate models. *Chinese J. Atmos. Sci.*, **34**, 323–336. (in Chinese)

Kalnay, E., and Coauthors, 1996: The NCEP/NCAR 40-year reanalysis project. *Bull. Amer. Meteor. Soc.*, **77**, 437–472.

Kiehl, J. T., and P. R. Gent, 2004: The Community Climate System Model, Version 2. *J. Climate*, **17**, 3666–3682.

Kistler, R., and Coauthors, 2001: The NCEP-NCAR 50-year reanalysis: Monthly means CD-ROM and documentation. *Bull. Amer. Meteor. Soc.*, **82**, 247–268.

Knutson, T. R., and S. Manabe, 1998: Model assessment of decadal variability and trends in the tropical Pacific Ocean. *J. Climate*, **11**, 2273–2296.

Kug, J.-S., K. P. Sooraj, F.-F. Jin, Y.-G. Ham, and D. Kim, 2011: A possible mechanism for El Niño-like warming in response to the future greenhouse warming. *International Journal of Climatology*, **31**, 1567–1572.

Lau, K. M., and L. Peng, 1987: Origin of low-frequency (intraseasonal) oscillations in the tropical atmosphere. Part I: Basic theory. *J. Atmos. Sci.*, **44**, 950–972.

Lau, K. M., and C. P. Chang, 1987: Planetary scale aspects of the winter monsoon and atmospheric teleconnections. *Monsoon Meteorology*, Chang and Krishnamurti, Eds., Oxford University Press, 161–202.

Li, C., 1990: Interaction between anomalous winter monsoon in East Asia and El Niño events. *Adv. Atmos. Sci.*, **7**, 36–46.

Li, J. P., and J. Wang, 2003: A modified zonal index and its physical sense. *Geophys. Res. Lett.*, **30**, doi: 10.1029/2003GL017441.

Li, Y., R. Lu, and B. Dong, 2007: The ENSO-Asian monsoon interaction in a coupled ocean-atmosphere GCM. *J. Climate*, **20**, 5164–5177.

Liu, H. L., X. H. Zhang, W. Li, Y. Yu, and R. Yu, 2004: An eddy-permitting oceanic general circulation model and its preliminary evaluations. *Adv. Atmos. Sci.*, **21**, 675–690.

Meehl, G. A., and W. M. Washington, 1996: El Niño-like climate change in a model with increased atmospheric CO_2 concentrations. *Nature*, **382**, 56–60.

Moss, R. H., and Coauthors, 2010: The next generation of scenarios for climate change research and assessment. *Nature*, **463**, 747–756.

Sun, B., and S. Sun, 1994: The analysis on the features of the atmospheric circulation in preceding winters for the summer drought and flooding in the Yangtze and Huaihe River Valley. *Adv. Atmos. Sci.*, **11**, 79–90.

Tao, S. Y., and J. Wei, 2008: Severe Snow and Freezing-Rain in January 2008 in the Southern China. *Climatic and Environmental Research*, **13**, 337–350. (in Chinese)

Taylor, K., R. Stouffer, and G. Meehl, 2009: A summary of the CMIP5 experiment design. [Available online at http://cmip-pcmdi.llnl.gov/cmip5/experiment_design.html.]

Thompson, D. W. J., and J. M. Wallace, 1998: The Arctic Oscillation signature in the wintertime geopotential height and temperature fields. *Geophys. Res. Lett.*, **25**, 1297–1300.

Wang, B., Z. Wu, C. P. Chang, J. Liu, J. Li, and T. Zhou, 2010: Another look at interannual-to-interdecadal variations of the East Asian winter monsoon: The northern and southern temperature modes. *J. Climate*, **23**, 1495–1512.

Wang, H. J., and D. B. Jiang, 2004: A new East Asian winter monsoon intensity index and atmospheric circulation comparison between strong and weak composite. *Quaternary Sciences*, **24**, 19–27. (in Chinese)

Wang, Y., and Coauthors, 2005: A new paleoenvironmental change proxy investigation in semi-arid and arid region of China. *Proc. IGARSS 2005: IEEE International Geoscience and Remote Sensing Symposium,* Vols. 1–8, Ieee, 5280–5282.

Wu, B., and J. Wang, 2002: Winter Arctic Oscillation, Siberian High and East Asian winter monsoon. *Geophys. Res. Lett.*, **29**, 1897, doi: 1810.1029/2002GL015373.

Wu, G., and Y. Zhang, 1998: Tibetan Plateau forcing and the timing of the monsoon onset over South Asia and the South China Sea. *Mon. Wea. Rev.*, **126**, 913–927.

Wu, G., H. Liu, Y. Zhao, and W. Li, 1996: A nine-layer atmospheric general circulation model and its performance. *Adv. Atmos. Sci.*, **13**, 1–18.

Yamaguchi, K., and A. Noda, 2006: Global warming patterns over the North Pacific: ENSO versus AO. *J. Meteor. Soc. Japan*, **84**, 221–241.

Yan, H. M., H. Yang, Y. Yuan, and C. Y. Li, 2011: Relationship between East Asian winter monsoon and summer monsoon. *Adv. Atmos. Sci.*, **28**, 1345–1356, doi: 10.1007/s00376-011-0014-y.

Yang, S., K. Lau, and K. Kim, 2002: Variations of the East Asian jet stream and Asian-Pacific-American winter climate anomalies. *J. Climate*, **15**, 306–325.

Ye, D. Z., and Y. X. Gao, 1979: *Tibetan Plateau Meteorology.* Science Press, Beijing, 279pp. (in Chinese)

Zhang, R., A. Sumi, and M. Kimoto, 1996: Impact of El Niño on the East Asian monsoon: A diagnostic study of the '86/87 and '91/92 events. *J. Meteor. Soc. Japan*, **74**, 49–62.

Zhao, J., Y. Cao, and J. Shi, 2010: Spatial variation of the Arctic Oscillation and its long-term change. *Tellus* (*A*), **62**, 661–672.

Zhou, T. J., R. C. Yu, Z. Z. Wang, and Q. Bao, 2005: *Impacts of Ocean-Land-Atmosphere Interactions over the East Asian Monsoon Region on the Climate in China.* Vol. 4, *Atmospheric Circulation Global Model* (*SAMIL*) *and the Coupled Model* (*FGOALS-s*). China Meteorological Press, 288pp. (in Chinese)

Zhou, W., C. Li, and X. Wang, 2007a: Possible connection between Pacific Oceanic interdecadal pathway and east Asian winter monsoon. *Geophys. Res. Lett.*, **34**, L01701, doi: 01710.01029/02006GL027809.

Zhou, W., X. Wang, T. J. Zhou, and J. C. L. Chan, 2007b: Interdecadal variability of the relationship between the East Asian winter monsoon and ENSO. *Meteor.*

Atmos. Phys., **98**, 283–293.

Zhou, W., J. C. L. Chan, W. Chen, J. Ling, J. G. Pinto, and Y. P. Shao, 2009: Synoptic-scale controls of persistent low temperature and icy weather over southern China in January 2008. *Mon. Wea. Rev.*, **137**, 3978–3991.

Zhu, Y., and H. Wang, 2010: The Arctic and Antarctic Oscillations in the IPCC AR4 Coupled Models. *Acta Meteorologica Sinica*, **24**, 176–188.